JCI insight

RESEARCH ARTICLE

Vimentin intermediate filament assembly regulates fibroblast invasion in fibrogenic lung injury

Ranu Surolia,[1] Fu Jun Li,[1] Zheng Wang,[1] Huashi Li,[1] Kevin Dsouza,[1] Vinoy Thomas,[2] Sergey Mirov,[3] Dolores Pérez-Sala,[4] Mohammad Athar,[5] Victor J. Thannickal,[1] and Veena B. Antony[1]

[1]Division of Pulmonary, Allergy, and Critical Care Medicine, Department of Medicine,[2]Department of Materials Science and Engineering, and [3]Department of Physics, University of Alabama at Birmingham (UAB), Birmingham, Alabama, USA. [4]Department of Structural and Chemical and Biology, Centro de Investigaciones Biológicas, Consejo Superior de Investigaciones Científicas (CSIC), Madrid, Spain. [5]Department of Dermatology, UAB, Birmingham, Alabama, USA.

Idiopathic pulmonary fibrosis (IPF) is a progressive disease, with a median survival of 3–5 years following diagnosis. Lung remodeling by invasive fibroblasts is a hallmark of IPF. In this study, we demonstrate that inhibition of vimentin intermediate filaments (VimIFs) decreases the invasiveness of IPF fibroblasts and confers protection against fibrosis in a murine model of experimental lung injury. Increased expression and organization of VimIFs contribute to the invasive property of IPF fibroblasts in connection with deficient cellular autophagy. Blocking VimIF assembly by pharmacologic and genetic means also increases autophagic clearance of collagen type I. Furthermore, inhibition of expression of collagen type I by siRNA decreased invasiveness of fibroblasts. In a bleomycin injury model, enhancing autophagy in fibroblasts by an inhibitor of VimIF assembly, withaferin A (WFA), protected from fibrotic lung injury. Additionally, in 3D lung organoids, or pulmospheres, from patients with IPF, WFA reduced the invasiveness of lung fibroblasts in the majority of subjects tested. These studies provide insights into the functional role of vimentin, which regulates autophagy and restricts the invasiveness of lung fibroblasts.

Introduction

Remodeling of the lung architecture is one of the hallmarks of idiopathic pulmonary fibrosis (IPF). Lung remodeling in IPF is characterized by intemperate, pathogenic invasion of fibroblasts and accumulation of extracellular matrix (ECM) proteins (1–3). Prior studies have emphasized the increased invasiveness of fibroblasts in animal models of pulmonary fibrosis and in the lungs of patients with IPF (4–9). Vimentin, an abundant cytoskeletal protein in cells of mesenchymal origin, has been associated with increased invasiveness (10). Mechanistically, vimentin provides cellular polarity to invading cells (11). A lack of vimentin is associated with defects in wound healing (12). Inhibiting vimentin protects from fibrotic injuries (13, 14), whereas overexpression of vimentin promotes increased invasiveness and excessive scarring (10). Our previous studies have demonstrated that modified forms of vimentin target signaling pathways that include transcription of profibrotic genes in pulmonary fibrosis (15, 16). However, the role of vimentin or its various forms in the development of an invasive phenotype of IPF fibroblasts has not been studied.

Autophagy is a homeostatic process that serves to degrade intracellular organelles and proteins; defects in this process may contribute to the pathogenesis of IPF (17–20). During autophagy, portions of the cytosol are sequestered inside autophagosomes that ultimately fuse with lysosomes for the degradation of entrapped cargo. Defective autophagy in IPF leads to impaired recycling of organelles and ECM proteins, such as collagen type I (18, 21–23). While cytoskeletal proteins such as actins may modulate autophagy initiation and trafficking of autolysosomes (24), the role of vimentin intermediate filaments (VimIFs) in the regulation of autophagy remains unclear.

Vimentin possesses a single cysteine residue, Cys328, which is crucial for its optimal organization and remodeling in cells (25). Targeting Cys328 can inhibit VimIF assembly. Withaferin A (WFA), a plant-derived alkaloid, binds to vimentin at Cys328 which is located in its conserved α-helix. The α-helix of vimentin lies

Conflict of interest: The authors have declared no conflict of interest.

Submitted: July 16, 2018
Accepted: February 26, 2019
Published: April 4, 2019.

Reference information: *JCI Insight*. 2019;4(7):e123253. https://doi.org/10.1172/jci.insight.123253.

in close proximity to the C-3 and C-6 sites of the first 2 rings in WFA. Covalent bonding of vimentin at the conserved α-helical coil domain inhibits its assembly and hence inhibits its organization into VimIFs (26).

In this study, we evaluated the role of VimIF in the altered autophagy and increased invasiveness of IPF fibroblasts.

Results

The periphery of fibrotic foci and IPF pulmospheres contain vimentin-rich cells. To identify the location of vimentin in IPF lung tissue, we immunostained IPF (n = 10) lung tissue sections for vimentin (Figure 1A). The signature morphologic lesion of IPF are fibrotic foci, which are multifocal sites of fibroproliferation in the lung (27). Vimentin was significantly upregulated at the periphery of fibrotic foci (Figure 1B). The cellular cuffs of fibrotic foci exhibited significantly increased vimentin expression as compared with the center of fibrotic foci ($P < 0.0001$) (Figure 1B).

Furthermore, pulmospheres prepared from primary cells obtained from IPF patient lung biopsies (n = 9) demonstrated a significantly greater number of vimentin-positive cells as compared with control pulmospheres from normal lung tissue (n = 8) ($P = 0.01$) (Figure 1, C and D). Together, these data demonstrate that vimentin expression is upregulated and localized at the edges of IPF lung fibrotic foci and pulmospheres.

Vimentin accumulates in IPF fibroblasts with deficient autophagy. IPF is a chronic disease related to aging; thus, the use of age-matched controls was crucial for our comparative studies. Serum starvation was used as an autophagy-inducing stress in fibroblasts to study comparative responses in age-matched controls and IPF subjects (Figure 2). Age-matched fibroblasts demonstrated no significant difference in vimentin expression between serum-starved and serum-supplemented conditions (Figure 2, A and B), whereas beclin 1 expression was upregulated in serum-starved conditions (Figure 2, A and C). Vimentin expression in IPF fibroblasts was increased in serum-starved conditions, with the presence multiple bands of vimentin (Figure 2A). Beclin 1 expression in IPF fibroblasts was unchanged in serum-starved conditions as compared with age-matched controls (Figure 2C). Serum-starved fibroblasts from age-matched controls showed increased autophagy, as indicated by increased levels of LC3BII (Figure 2, A and D). This increase was not observed in serum-starved IPF fibroblasts (Figure 2, A and D). Overall, serum starvation triggered autophagy in control fibroblasts but not in IPF fibroblasts. Serum starvation also increased vimentin expression exclusively in IPF fibroblasts.

To study the functional implications of autophagic resistance and increased vimentin expression on fibroblast invasion, we utilized 3D pulmospheres to measure cellular invasiveness. IPF pulmospheres (n = 5 patients) had a higher percent zone of invasion as compared with pulmospheres obtained from age-matched subjects (n = 5) (138.2% ± 17.88 % vs. 83.99% ± 6.77%, respectively). The pulmospheres from IPF patients were more invasive upon serum starvation (138.2 ± 17.88 vs. 180.2 ± 6.34 respectively), whereas serum-starved pulmospheres from age-matched control subjects demonstrated no significant difference in invasiveness as compared with serum-supplemented pulmospheres (Figure 2E). Immunostaining for vimentin in control and IPF pulmospheres established that most vimentin-positive cells were localized in the periphery of pulmospheres and in the zone of invasion. Serum starvation caused a mild increase in vimentin-positive cells in pulmospheres from age-matched control (4.1% to 5.5%) and IPF (10.8% to 32.7%) subjects as compared with their counterparts in complete medium (Figure 2, F and G). The photomicrograph of a single invasive cell demonstrates the differential organization of vimentin filaments in controls and IPF fibroblasts (Figure 2G). Fibroblasts from age-matched controls demonstrated a differential morphology of vimentin in the presence or absence of serum. VimIFs were present in serum-starved conditions, whereas in serum-supplemented conditions, vimentin had a predominant morphology of dots or squiggles at the cell edge. In contrast, in IPF fibroblasts, vimentin consisted of long intermediate filament bundles under both conditions. Serum-starved IPF fibroblasts organized VimIFs that extended to the invading edge of the fibroblast (Figure 2H).

Inhibition of VimIF assembly by WFA induces autophagy in IPF fibroblasts. Since VimIF pools were upregulated in autophagy-resistant IPF fibroblasts, we tested the effect of inhibition of VimIF assembly on autophagy. WFA inhibits VimIF assembly (26). Transmission electron microscopy images demonstrated an increase in autophagic vacuoles in WFA-treated IPF fibroblasts compared with vehicle-treated cells (Figure 3A). Immunostaining for LC3B antibody demonstrated increased formation of LC3BII puncta (Figure 3B). Western blot analysis of vimentin showed a reduction in the intensity of the band corresponding to the intact protein (Figure 3, C and D), together with an increase in the levels of vimentin fragments (Figure 3C). Similarly, Western blotting confirmed upregulation of LC3BII and beclin 1 expression in treated fibroblasts (Figure 3, C, E, and F).

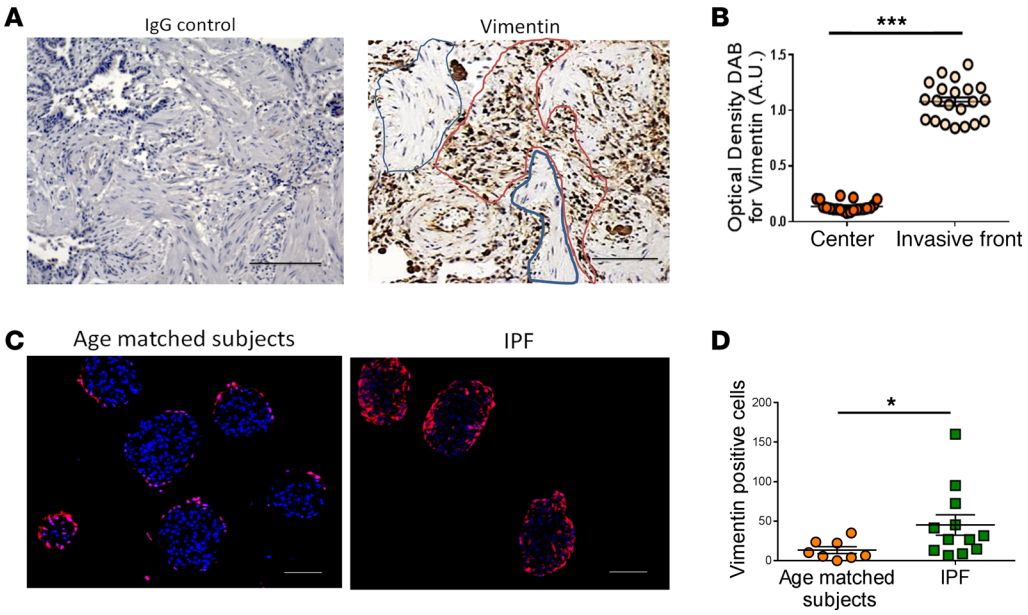

Figure 1. Vimentin expression is upregulated at the margins of IPF fibrotic foci. (**A**) IHC staining showing IgG control and expression of vimentin in formalin-fixed, paraffin-embedded tissue section of a representative subject with IPF. Scale bars: 100 μm. Area outlined in red is the invasive front of fibrotic foci (outlined in blue). (**B**) Quantification of DAB-positive vimentin-expressing cells in the center and at the cellular cuffs of fibrotic foci. Graph shows representative results for an individual subject (n = 5). Each dot represents DAB intensity per area. Data are represented as mean ± SD. (**C**) Representative image of the expression of vimentin in pulmospheres obtained from the cells isolated from control and IPF lung tissue. The pulmospheres were seeded for an hour in collagen gel prior to immunostaining for vimentin (red). Nuclei were stained with DAPI (blue). Scale bars: 100 μm. (**D**) Quantification of vimentin-positive cells in pulmospheres from controls and IPF subjects. Data are represented as mean ± SD. Each dot represents an individual subject. $^{*}P < 0.05$, $^{***}P < 0.001$.

To determine autophagic flux, we tested the effect of chloroquine (10 μM) on WFA treatment of IPF fibroblasts. Enhanced LC3BII formation was observed in fibroblasts cotreated with WFA and chloroquine, which suggested an increase in autophagic flux by WFA (Figure 3G). A tandem autophagy sensor fluorescent label (RFP-GFP-LC3B) was used, where once the autophagosome fuses with the lysosome, the pH change quenches GFP, making the autophagosome appear red. Chloroquine-treated cells showed puncta positive for autophagosome accumulation, indicated by their yellow color (red and green overlap) as the result of absence of fusion of autophagosomes to lysosomes. This represents a positive control for disrupted autophagic flux. WFA-treated fibroblasts showed red puncta due to the fusion of autophagosome with lysosomes and increased autophagic flux (Figure 3H). Overall, WFA treatment elicited intense disruption of VimIF organization and triggered autophagy in IPF fibroblasts.

WFA-regulated autophagy is beclin 1 dependent. Based on our finding that WFA treatment increases beclin1 expression in IPF fibroblasts (Figure 3C), we explored whether beclin 1 is required for WFA-induced autophagy in IPF fibroblasts. Downregulation of beclin 1 with siRNA-mediated silencing not only markedly diminished WFA-induced autophagy in transfected fibroblasts — as deduced from the lower LC3BII levels (Figure 4A) — but also potentiated effects of TGF-β1 on collagen type I expression, although vimentin expression was not altered (Figure 4B). When beclin 1 was silenced in IPF pulmospheres, fibroblasts were rearranged mostly in the periphery of the pulmospheres. Beclin 1–silenced pulmospheres were highly invasive as compared with those in the control pulmospheres (Figure 4C).

To delineate the interaction between beclin 1 and VimIFs, we performed immunoprecipitation studies and demonstrated that vimentin coimmunoprecipitated with beclin 1 and WFA treatment significantly reduced the binding of beclin 1 to vimentin. Whole cell lysate immunoblots demonstrated increased LC3BII and beclin 1 and decreased vimentin levels with WFA treatment (Figure 4D). Beclin 1 localized with vimentin in vehicle-treated fibroblasts. Furthermore, WFA treatment resulted in the less overlap of beclin 1 and vimentin staining (Figure 4E).

WFA-induced VimIF disruption increases collagen type I turnover in autophagosomes in IPF fibroblasts. To study the antifibrotic effects of enhanced autophagy by VimIF disruption, we assessed protein levels of collagen

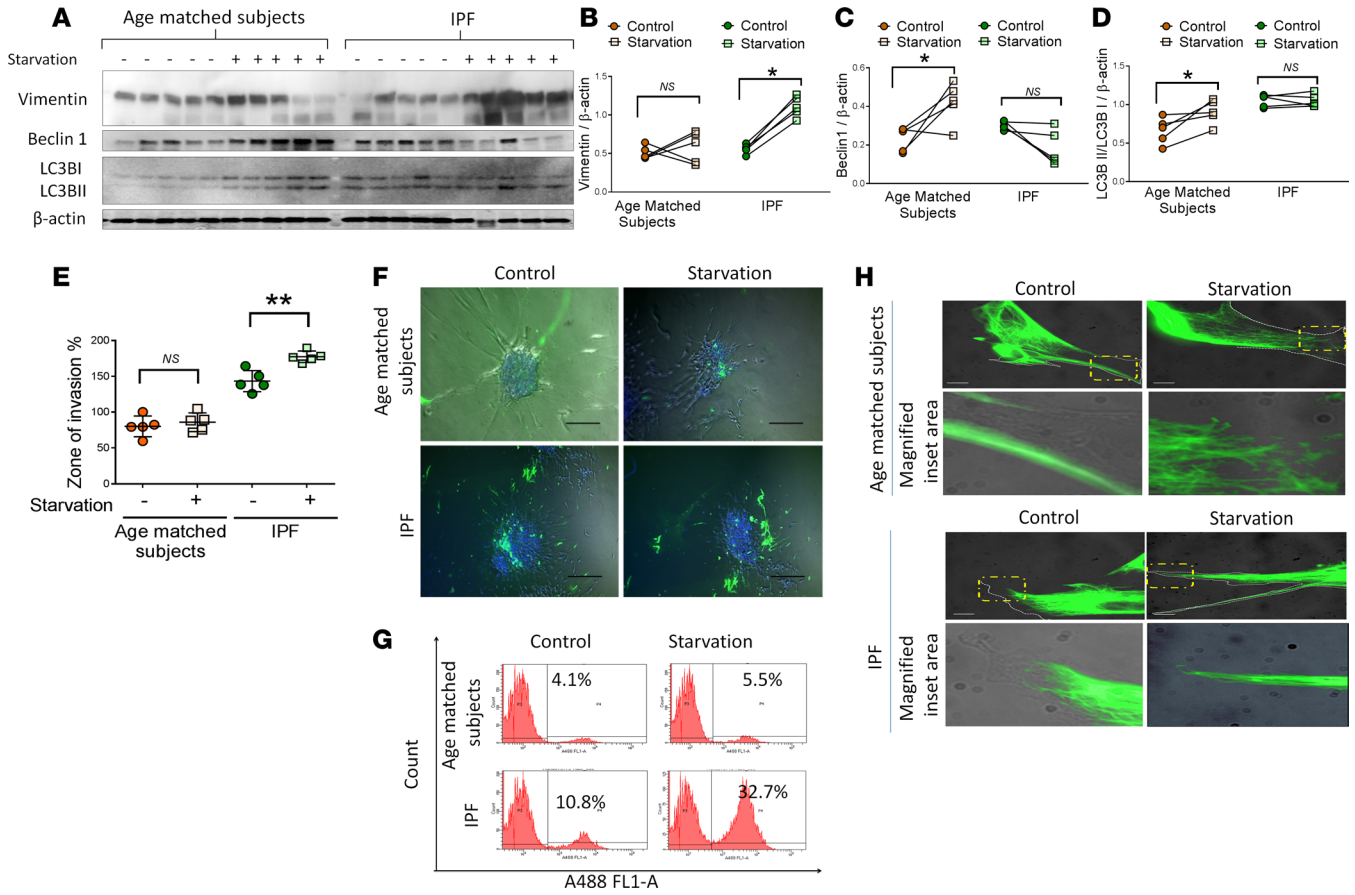

Figure 2. Vimentin expression is upregulated during attenuated autophagy in IPF fibroblasts. (**A**) Immunoblot analysis of vimentin and the autophagic markers beclin 1 and LC3BII in cell lysates of fibroblasts from age-matched subjects (n = 5) and IPF (n = 5) lung tissue in complete medium (control) and serum-starved conditions. β-Actin served as loading control. Densitometry analysis of protein expression in Western blot for (**B**) vimentin, (**C**) beclin 1, and (**D**) LC3BII/LC3BI normalized with β-actin in controls and IPF fibroblasts. *P < 0.05. (**E**) Invasiveness in the pulmospheres obtained from age-matched subjects and IPF lung in complete medium and serum-starved conditions. Data are presented as mean ± SD; each dot represents an individual patient. **P < 0.01. Vimentin expression in complete medium and serum-starved conditions in pulmospheres from age-matched subjects and IPF patients (**F**) (scale bars: 200 μm); quantitation by FACS analysis of vimentin-positive cells in dissociated pulmospheres (**G**). (**H**) Single invasive fibroblast in pulmospheres (scale bars: 10 μm).

type 1 after WFA treatment of IPF fibroblasts. WFA treatment resulted in decreased expression of vimentin and collagen type I in a time-dependent manner (Figure 5, A and B). The maximum inhibition of collagen type I was observed at the 24-hour time point. Immunofluorescence staining of WFA-treated IPF fibroblasts also showed reduced intensity of collagen type I compared with controls. Immunostaining of WFA-treated IPF fibroblasts showed overlapping staining of LC3BII (green; indicating autophagosomes) and collagen type I (Figure 5C), which suggested autophagic degradation of collagen type I.

To assess whether induction of autophagy inhibits invasiveness of IPF fibroblasts, we used an inhibitor, chloroquine, and an inducer, rapamycin, to treat IPF pulmospheres. Chloroquine increased the invasiveness of IPF fibroblasts, whereas rapamycin inhibited the invasiveness of IPF fibroblasts (Figure 5D). Furthermore, to check the direct effect of collagen type I on the invasiveness of fibroblasts, we transfected IPF fibroblast with siCOL1. Collagen type I expression was decreased in fibroblasts treated with WFA, collagen I siRNA (siCOL1), and WFA plus siCOL1 as compared with nontargeted control siRNA (siNT) (Figure 5E). These fibroblasts were used to prepare pulmospheres as described, and pulmospheres were evaluated for invasiveness. siCOL1 treatment decreased the invasiveness of IPF pulmospheres. The cotreatment with WFA further decreased invasiveness of fibroblasts (Figure 5F).

WFA-treated pulmospheres had decreased expression of collagen type I (~2 fold), as shown in Figure 5G. Supernatants of IPF fibroblasts tested for soluble collagen by the Sircol assay showed significantly decreased levels of soluble collagen after WFA treatment (Figure 5H). In summary, these data suggest that

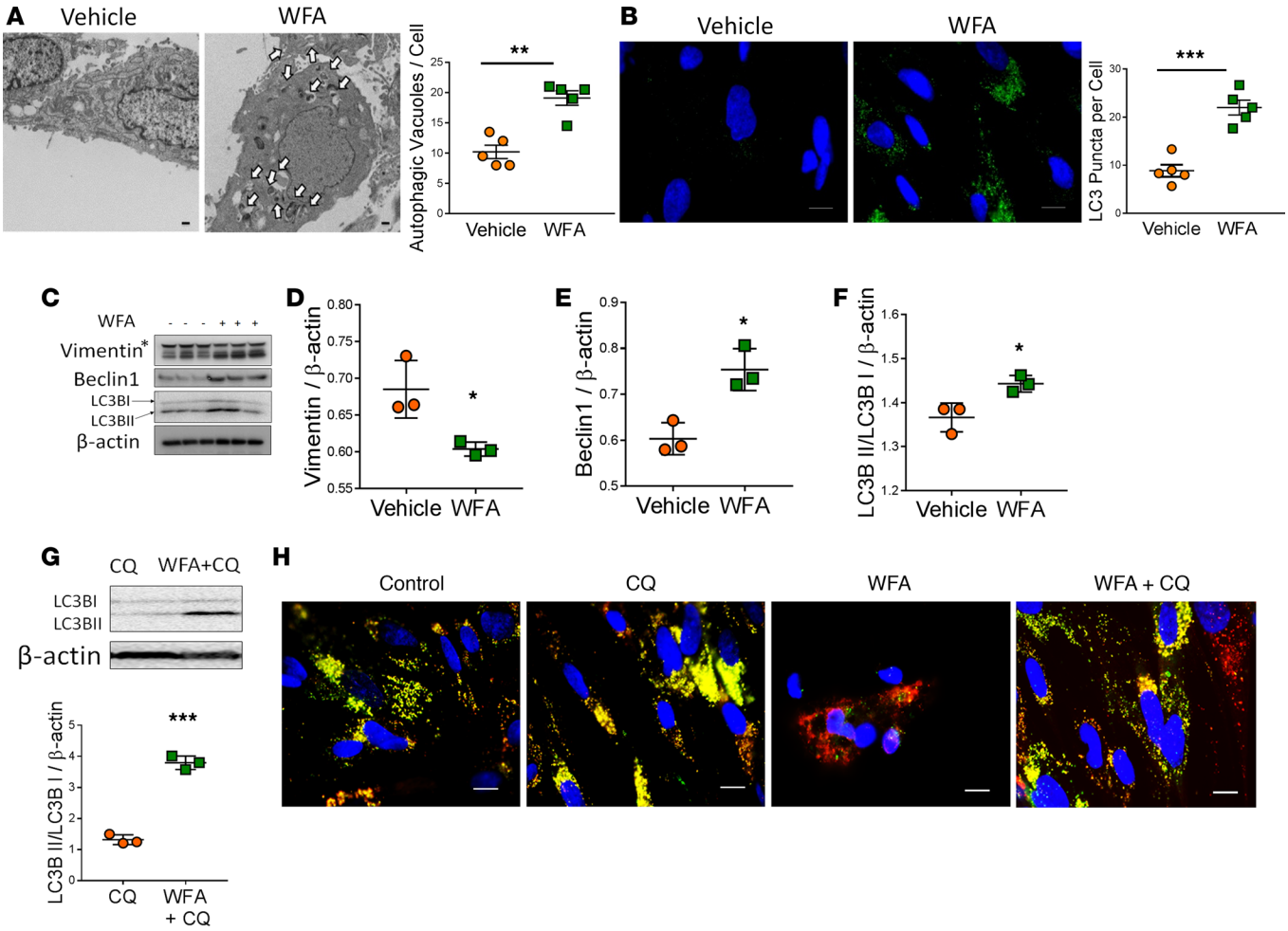

Figure 3. Inhibition of VimIF assembly induces autophagy in IPF fibroblasts. (**A**) Representative electron photomicrograph and quantitative graph showing increased number of autophagic vacuoles in vehicle and WFA-treated IPF fibroblasts. Data are presented as mean ± SEM. Three cells per IPF patient were analyzed for the quantification of autophagic vacuoles. Each dot represents an individual patient. $^{**}P < 0.01$, as compared with vehicle-treated fibroblasts. Scale bars: 10 μm. (**B**) Human fibroblasts were treated with vehicle or WFA, and laser confocal microscopy was performed to detect LC3B by indirect immunofluorescence. Nuclei were costained with DAPI (blue). Scale bars: 20 μm. Graph represents the quantification of LC3BII puncta in WFA-treated fibroblasts. $^{***}P < 0.001$, as compared with vehicle-treated fibroblasts. Data are mean ± SD ($n = 5$ patients). (**C**) Immunoblot analysis for vimentin, LC3B, and beclin 1 of cell lysates from WFA-treated IPF fibroblasts. Asterisk indicates vimentin 56-kDa band. Each lane represents an individual subject. β-Actin served as loading control. Densitometry for (**D**) vimentin (band at 56 kDa), (**E**) beclin 1, and (**F**) LC3BII/LC3B I ratio normalized to β-actin for the Western blot. $^{*}P < 0.05$, compared with vehicle-treated fibroblasts. (**G**) Immunoblot analysis for LC3B of cell lysates from IPF fibroblasts treated with chloroquine (CQ) and cotreated with WFA/CQ. β-Actin served as loading control. Data are representative of 3 experiments. The graph represents densitometry analysis for LC3BII/LC3B I ratio normalized to β-actin for the immunoblot blot analysis of LC3B. $^{***}P < 0.001$, compared with vehicle-treated fibroblasts. (**H**) Representative images of cells expressing the RFP-GFP-LC3B construct followed by the treatment with vehicle alone (control) or CQ, WFA, and WFA/CQ cotreatment for 12 hours. CQ-treated cells served as a positive control. Nuclei were costained with DAPI (blue). Natural-pH LC3B-positive autophagosome (green fluorescence) and acidic-pH LC3B-positive autophagolysosome (red fluorescence) were detected respectively using a fluorescence microscope. Scale bars: 20 μm

the antifibrotic and anti-invasive effects of WFA in IPF fibroblasts could be due, in part, to inhibition of collagen type I expression and its clearance via autophagy.

WFA protects from lung fibrosis through increased autophagy in vivo. To define the in vivo role of VimIFs in the reparative response to fibrotic injury in mammalian lung, we used a murine model of bleomycin-induced fibrotic lung injury (28). WFA was administered intraperitoneally (2 mg per kg body weight) every day from day 10 to day 21 after bleomycin exposure (Figure 6A). Mice were sacrificed on day 21. WFA induced autophagy in the lungs of bleomycin-treated mice, as evidenced by observation of LC3BII (autophagic form of LC3B) puncta (Figure 6B). Quantitation of the punctate form of LC3BII intensity by ImageJ software confirmed increased autophagy in WFA-treated bleomycin-administered mice (Figure 6C). WFA alone demonstrated no substantial effect on expression levels of beclin 1, LC3B, and p62 when compared with saline-treated mice

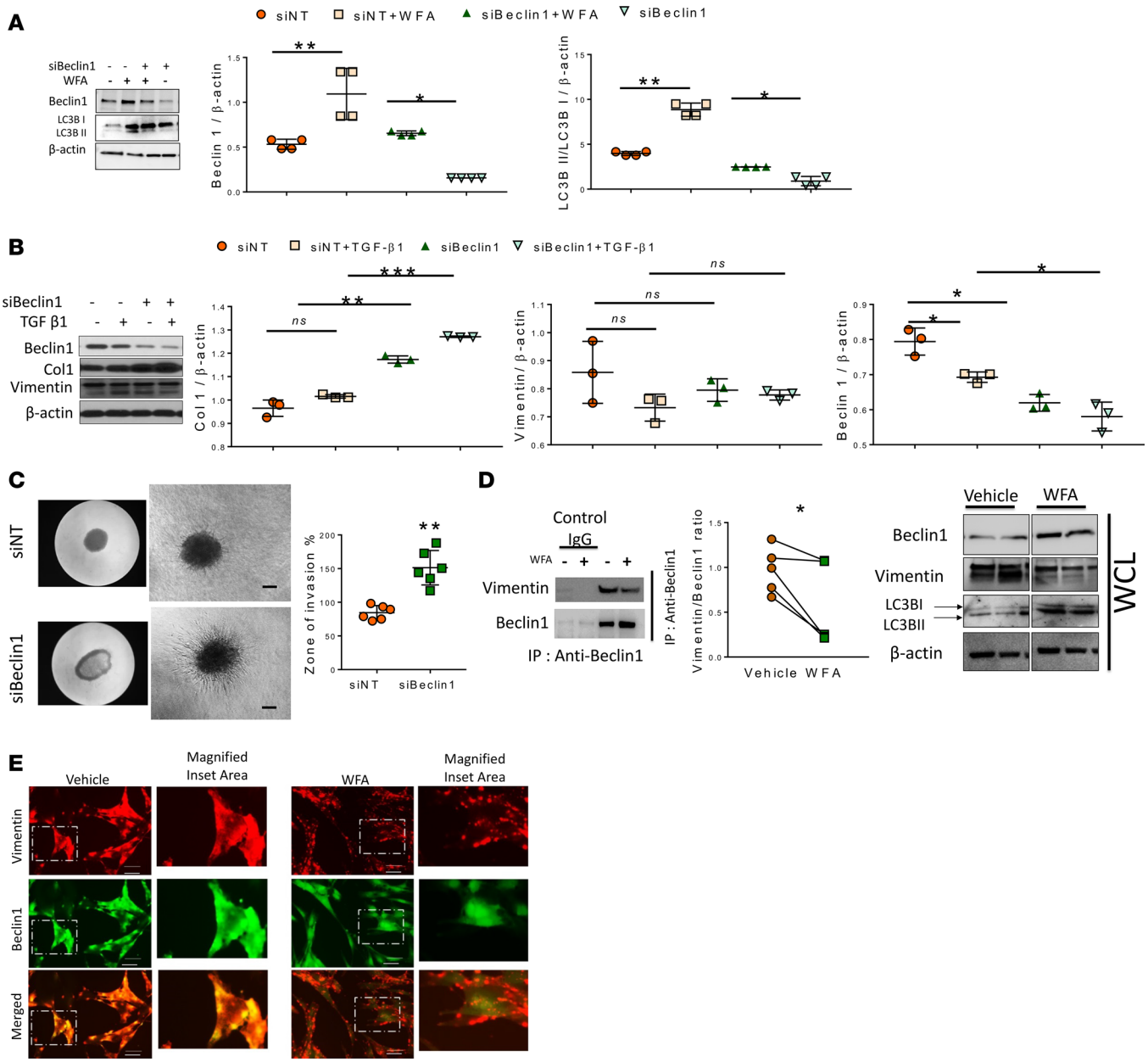

Figure 4. WFA-regulated autophagy is beclin 1 dependent. (**A**) Immunoblot analysis and densitometry for beclin 1 and LC3B of cell lysates from nontargeted siRNA– and beclin 1 siRNA–transfected (siNT- and siBeclin1-transfected) IPF fibroblasts treated with WFA. β-Actin served as loading control. Data are representative of 3 experiments. (**B**) Immunoblot analysis and densitometry of collagen I (Col1), vimentin, and beclin 1 from cell lysates from siNT- and siBeclin1-transfected IPF fibroblasts treated with WFA. β-Actin served as loading control. Data are representative of 3 experiments. $^{*}P < 0.05$, $^{**}P < 0.01$, $^{***}P < 0.001$. (**C**) Representative image and measurement of invasiveness (percent zone of invasion) in beclin 1 siRNA–transfected IPF pulmospheres. siNT was used as control. Scale bars: 100 μm. $^{**}P < 0.01$, compared with siNT fibroblasts. (**D**) Immunoprecipitation studies with anti–beclin 1 antibodies of cell lysates from IPF fibroblasts treated with vehicle and WFA. The graph represents vimentin/beclin 1 binding ratio. Precipitates were immunoblotted for associated beclin 1 and vimentin, and whole cell lysates (WCL) for LC3B, vimentin, and beclin 1 antibodies. β-Actin served as loading control for cell lysates. (**E**) Immunostaining for beclin 1 (green) and vimentin (red) in IPF fibroblasts treated in the absence or presence of WFA. Scale bars: 20 μm.

(control), as revealed by Western blot analysis. Treatment with WFA downregulated vimentin expression in the lungs of bleomycin-administered mice as compared with control mice that were treated with either WFA alone or bleomycin alone (Figure 6, D and E). Densitometry demonstrated no significant effect on the expression of vimentin in only WFA–treated mouse lungs (Figure 6E). Treatment with WFA upregulated beclin 1 and LC3B expression in the lungs of bleomycin-administered mice relative to control mice (WFA and bleomycin alone). p62 accumulation demonstrated reduced autophagic flux, whereas WFA treatment in bleomycin-administered mice demonstrated p62 clearance and increased autophagic flux (Figure 6, D and E).

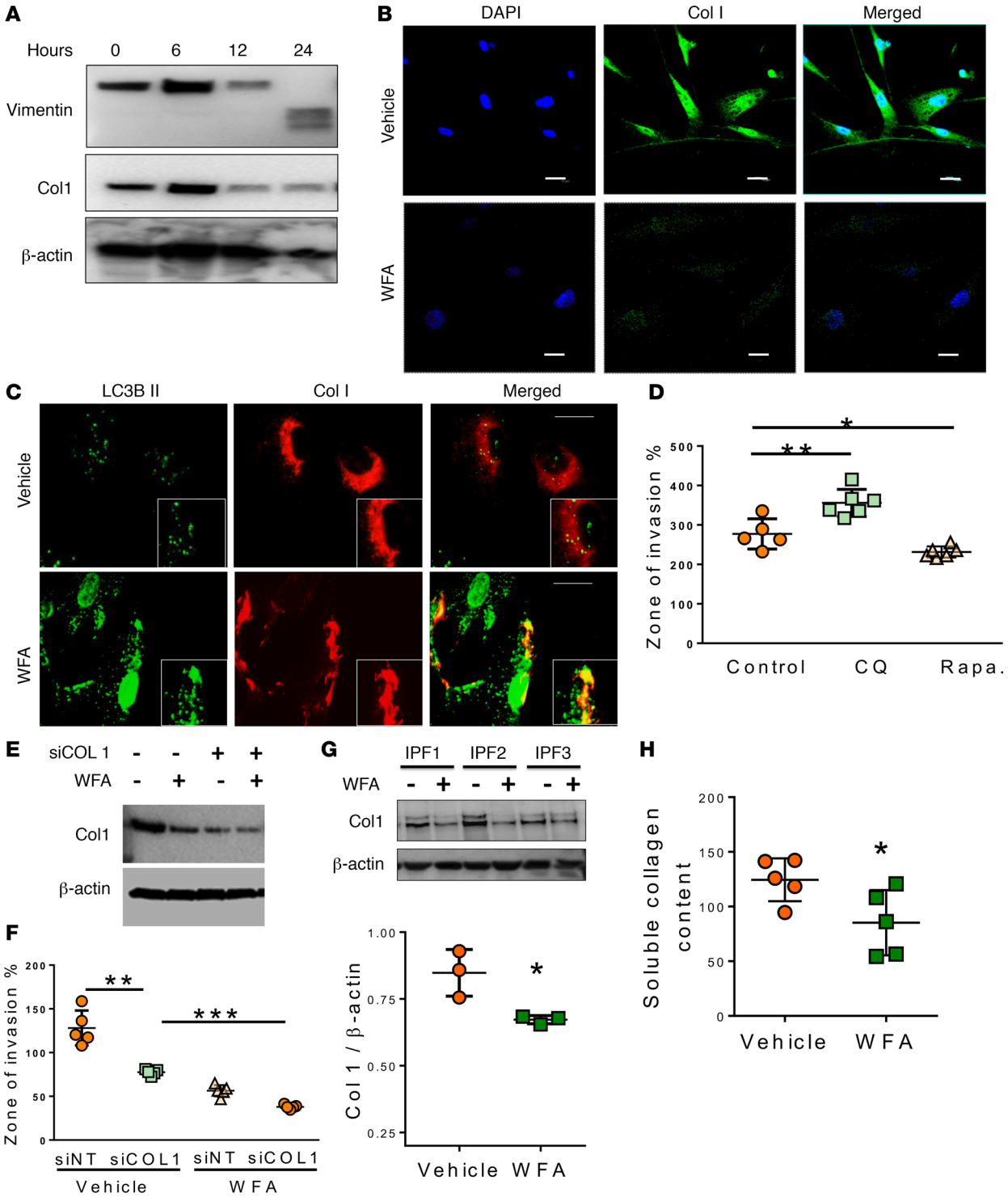

Figure 5. Inhibition of VimIF assembly induces autophagic clearance of collagen type I in IPF fibroblasts. (**A**) Immunoblot analysis for vimentin and collagen type I (Col I) on cell lysates of IPF fibroblasts treated with WFA for different durations. β-Actin served as loading control. Data are representative of 3 experiments. (**B**) Immunostaining for Col I in IPF fibroblasts treated with vehicle (control) or WFA. Nuclei were costained with DAPI. Scale bars: 20 μm. (**C**) IPF fibroblasts were treated with vehicle (control) or WFA, and the presence of Col I in autophagosomes was assessed by indirect immunofluorescence and visualization of Col I– and LC3B-positive structures by immunofluorescence microscopy. Scale bars: 20 μm. Inset box shows magnified area of interest. (**D**) Measurement of invasiveness (percent zone of invasion) in IPF patient pulmospheres after treatment with an autophagy inhibitor (chloroquine [CQ]) or autophagy inducer (rapamycin [Rapa.]). Each dot represents an individual patient. $*P < 0.05$, $**P < 0.01$, as compared with control. (**E** and **F**) Immunoblot of Col I siRNA– transfected (siCOL1) human fibroblasts and measurement of invasiveness (zone of invasion percent) in IPF pulmospheres after siCOL1 transfection in the presence or absence of WFA. $**P < 0.005$, $***P < 0.001$. (**G**) Fibroblasts from IPF subjects were treated with WFA to evaluate the expression of Col I. β-Actin served as loading control. (**H**) Quantification of soluble collagen in the supernatants of IPF fibroblasts treated with vehicle (control) or WFA. $*P < 0.05$, compared with vehicle-treated fibroblasts.

Measurements of invasiveness in pulmospheres prepared from mouse lung cells treated with vehicle, WFA, bleomycin, and bleomycin/WFA demonstrated increased zone of invasion in bleomycin-treated mice as compared with pulmospheres from vehicle-treated and WFA-treated mouse lungs. There was no significant difference in the invasiveness of WFA only–treated mouse lung pulmospheres. Cotreatment with WFA further decreased the zone of invasion (Figure 6F). Overall, these data suggest that WFA augments autophagy in the lungs of bleomycin-injured mice and decreases invasiveness of fibroblasts. Immunostaining of mouse lung pulmospheres prepared from bleomycin-administered mice demonstrated faint LC3B staining and several vimentin-positive invasive cells. The pulmospheres prepared from bleomycin/WFA-cotreated mouse lung cells demonstrated increased LC3B at the periphery of pulmospheres and fewer invasive cells (Figure 6G).

MicroCT images demonstrated increased lung density following bleomycin treatment. WFA-treated bleomycin-exposed mice had decreased lung tissue density as compared with vehicle-treated bleomycin-exposed mice (Figure 6H). H&E staining and IHC staining for collagen type I and Picrosirius red confirmed a protective role for WFA in bleomycin-induced fibrotic lung injury. Overall collagen levels (Picrosirius red staining) and specifically collagen type I (IHC staining) levels were decreased (Figure 6I) in WFA-treated bleomycin-administered mouse lungs. Hydroxyproline assay analysis on day 21 demonstrated decreased hydroxyproline content in WFA-treated bleomycin-exposed mice as compared with vehicle-treated bleomycin-exposed mice. There was no significant difference in hydroxyproline content in control and WFA only–treated mice (Figure 6J). Collectively, these data demonstrate that WFA promotes autophagy and protects from bleomycin-induced fibrotic lung injury.

Inhibition of VimIFs decreases invasiveness of IPF fibroblasts. Since fluorescent WT or C328S constructs can incorporate into a normal network in cells expressing endogenous vimentin, we used $Vim^{-/-}$ mouse fibroblasts for the transfections. VimIF-associated effects on autophagy were studied in Vim-C328S vimentin–transfected fibroblasts (lacking the ability to assemble VimIFs) isolated from $Vim^{-/-}$ mouse lungs. Fluorescence images of WT fibroblasts demonstrated the presence of vimentin intermediate filaments, and the C328S fibroblasts showed the presence of squiggles and dots like structures of vimentin (Figure 7A). C328S fibroblasts demonstrated higher expression of LC3BII as compared with WT fibroblasts upon serum starvation (Figure 7B). There was no significant difference in vimentin expression (Figure 7B). Immunostaining for LC3B in WT fibroblast pulmospheres demonstrated a diffuse cytosolic form of LC3B; however, C328S fibroblast pulmospheres demonstrated increased LC3B staining intensity (Figure 7C). These images clearly demonstrate more invasive fibroblasts in WT pulmospheres when compared with C328S pulmospheres (Figure 7C). The effect of WFA treatment on invasiveness of fibroblasts was evaluated in 3D pulmosphere from patients with IPF. Fluorescence images of mEmerald-vimentin plasmid–transfected IPF pulmospheres demonstrated a less-filamentous structure of vimentin in invasive cells after WFA treatment as compared with vehicle-treated pulmospheres (Figure 7D). WFA treatment significantly decreased invasiveness of pulmospheres (Figure 7E). Transmission electron microscopy pictures of pulmospheres demonstrated the presence of autophagic vacuoles in invasive cells and provided direct evidence that WFA treatment result in increased autophagy in invasive cells (Figure 7F).

Pulmospheres prepared from 15 IPF patient lung biopsies were tested for the anti-invasive effect of WFA. Untreated pulmospheres from each subject served as controls. The fold change in zone of invasion was calculated as shown in Figure 7G. A decrease in fold change ratio of less than 1 demonstrated a decrease in zone of invasion of pulmospheres after treatment with WFA as compared with the zone of invasion of untreated pulmospheres obtained from an individual IPF patient. Fourteen of 15 patient pulmospheres demonstrated inhibition of invasion following WFA treatment (Figure 7H).

Discussion

Fibroblast invasion and deposition/remodeling of the ECM are hallmarks of IPF (1, 9, 29, 30). In this study, we demonstrate the dual effects of increased VimIFs in IPF fibroblasts — on their capacity for invasion as well as ECM turnover. We used WFA to bind and disrupt VimIFs (26). WFA interacts with the Cys328 amino acid of vimentin and inhibits its polymerization into VimIFs (26). Our results demonstrate that WFA disrupts vimentin filament assembly and promotes autophagy. We assessed the effect of WFA treatment in normal fibroblasts at the dose of 1 μmol for 3- to 12-hour time points. We found that WFA had enhanced specificity toward VimIF disruption and autophagy induction in IPF fibroblasts. WFA did not alter VimIFs and autophagy in normal fibroblasts (Supplemental Figures 1 and 2; supplemental material available online with this article; https://doi.org/10.1172/jci.insight.123253DS1).

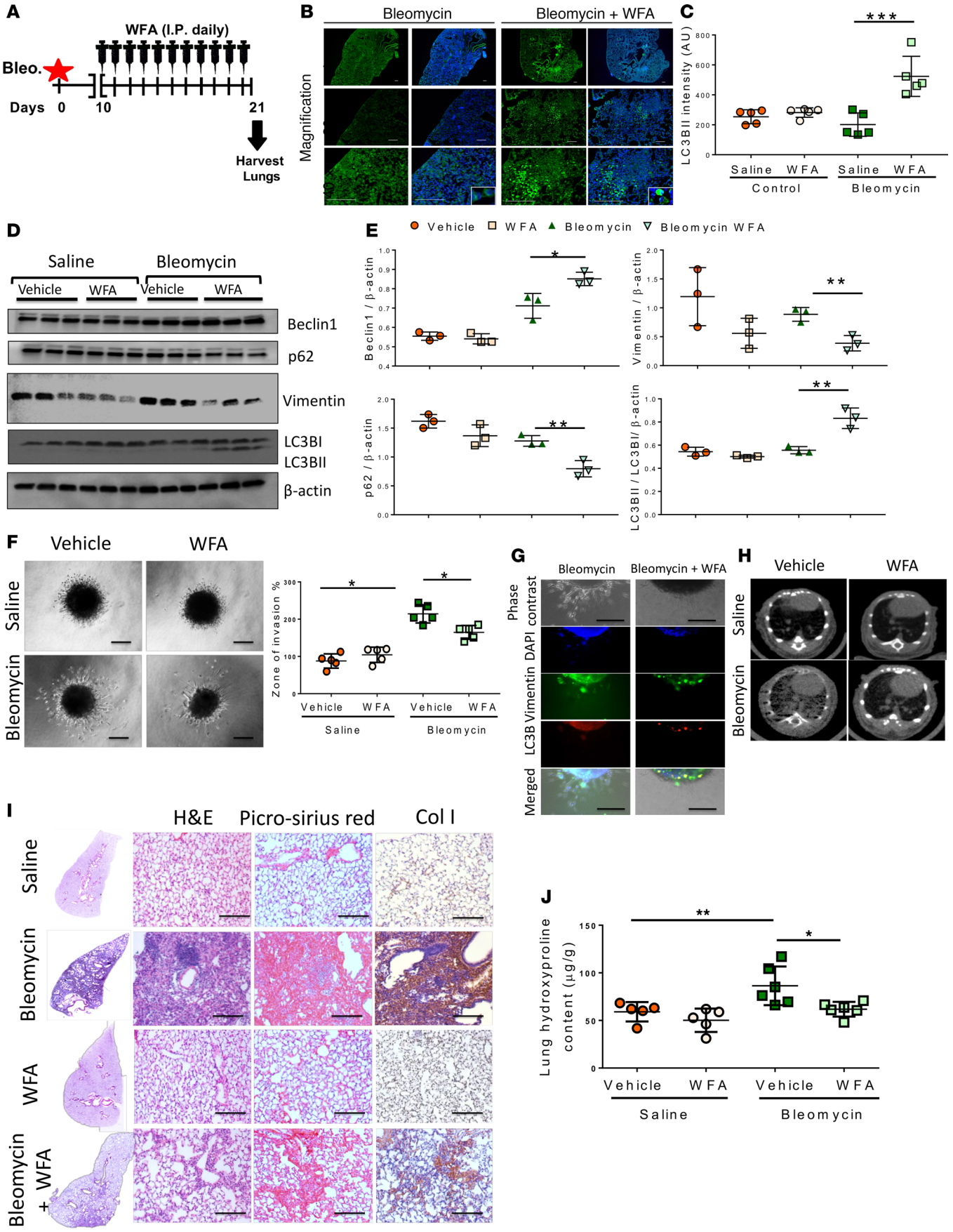
A
WFA (I.P. daily)
Bleo.
Days 0 10 21
Harvest Lungs
B
Bleomycin
Bleomycin + WFA
Magnification
C
LC3BII intensity (AU)
Saline WFA Saline WFA
Control Bleomycin
D
Saline Bleomycin
Vehicle WFA Vehicle WFA
Beclin1
p62
Vimentin
LC3BI
LC3BII
β-actin
E
Vehicle WFA Bleomycin Bleomycin WFA
Beclin1 / β-actin
Vimentin / β-actin
p62 / β-actin
LC3BII / LC3BI/ β-actin
F
Vehicle WFA
Saline
Bleomycin
Zone of invasion %
Vehicle WFA Vehicle WFA
Saline Bleomycin
G
Bleomycin Bleomycin + WFA
Phase contrast
DAPI
Vimentin
LC3B
Merged
H
Vehicle WFA
Saline
Bleomycin
I
H&E Picro-sirius red Col I
Saline
Bleomycin
WFA
Bleomycin + WFA
J
Lung hydroxyproline content (μg/g)
Vehicle WFA Vehicle WFA
Saline Bleomycin

Figure 6. WFA protects from pulmonary fibrosis in bleomycin mice model. (**A**) Schematic of animal model and WFA treatment (**B**) LC3B II puncta formation, as assessed by immunofluorescence staining for LC3B (green) and nuclei (DAPI, blue) in paraffin embedded mouse lung sections on day 21. Scale bar: 100 μm. Bleo., bleomycin. (**C**) Quantification of intensity of LC3BII puncta in immunofluorescently labeled mouse lung sections by ImageJ. (**D**) Immunoblot analysis and (**E**) densitometry for beclin 1, p62, vimentin, and LC3B in whole lung homogenates from C57BL/6 mice subjected to control saline, bleomycin, WFA, and bleomycin and WFA treatment on day 21. β-Actin served as loading control. Data are representative of 3 experiments. (**F**) Representative images and measurement of invasiveness (zone of invasion percent) in pulmospheres prepared from lung cells from C57BL/6 mice subjected to control saline, bleomycin, WFA and bleomycin/WFA on day 21. Scale bars: 100 μm. (**G**) Representative images of immunofluorescence staining for vimentin (green), LC3B (red), and nucleus (DAPI, blue) in pulmospheres prepared from mouse lungs cells after 21 days of bleomycin and bleomycin/WFA exposure. Scale bar: 50 μm (**H**) MicroCT analysis of mouse lungs on day 20. (**I**) Fibrosis, as assessed on day 21 by H&E staining. Collagen deposition was analyzed using Picrosirius staining and IHC analysis of Col 1. Scale bar: 100 μm. (**J**) Lung homogenates analyzed on day 21 for hydroxyproline content. Values represent means ±SD, $n = 5$. $^{*}P < 0.05$, $^{**}P < 0.01$, $^{***}P < 0.001$.

Vimentin is a dynamic type III intermediate filament, cytoskeletal protein (31). Structurally, vimentin is a coiled-coil protein composed of central α-helical regions linked by connecting segments and flanked by disordered head and tail domains. Vimentin particles fuse into structures known as short squiggles, which are soluble, that can assemble in a nonpolar fashion into the elongated form of vimentin intermediate filaments, which are insoluble (32). The interchangeable dynamics of soluble vimentin and assembly of VimIFs are important for the cellular movement of fibroblasts (33–37). Soluble vimentin has been shown to localize in lamellipodia, which are important for cell migration (36). On the other hand, VimIFs are essential for cellular invasion through ECM and the elongation of invasive invadopodia (37). Invadopodia are special F-actin protrusions containing VimIFs present in invading cells that arise on the internal surface of cell membranes (38). Loss of vimentin leads to loss of polarity and loss of the capacity to invade (39). Consistent with other studies, our data demonstrate that the dynamics of VimIF assembly are equally important as vimentin levels in regulating cellular invasiveness (37, 40).

Dysfunctional autophagy has been previously reported in IPF (18–21). A number of studies have highlighted the signaling pathways involved in VimIF interaction with autophagy regulatory proteins (41, 42). The role of VimIFs in regulation of autophagic homeostasis in IPF fibroblasts is not known. Total vimentin expression is increased during dysfunctional autophagy in IPF fibroblasts. A possible reason is that defective autophagy increases cellular stress that, in turn, further induces vimentin expression and VimIF assembly (43–45). Our data demonstrate that VimIFs associate with beclin 1 to form a VimIF–beclin 1 complex, which is known to inhibit autophagy (42, 46). Endogenous beclin1 coimmunoprecipitated with vimentin. Blocking formation of VimIFs with WFA decreased this interaction. Beclin 1 interacts with vimentin via 14-3-3 to regulate autophagy through AKT signaling (42). We recently demonstrated that AKT- and cdc2-mediated increased interaction of 14-3-3 with vimentin in the development of peribronchial fibrosis (16). The interaction of 14-3-3 with beclin 1 and vimentin is well established (42, 47–49). Beclin 1 siRNA studies in IPF fibroblasts provided evidence that WFA-induced autophagy is beclin 1 dependent. Taken together, our results show, for the first time to our knowledge, that the increased association of VimIFs and beclin 1 decreases autophagy in IPF fibroblasts.

Collagen type I, a component of ECM, is abundantly secreted by IPF fibroblasts at the site of lung tissue remodeling (50). Increased ECM deposition and tissue stiffening in IPF act as a potent profibrotic stimulus that further enhances expression of collagen type I (51). WFA decreased levels of collagen type I. First, inhibition of VimIF assembly hinders the stabilization of collagen mRNA by decreasing its half-life (52). Second, the greater availability of beclin 1 due to decreased interaction with VimIF results in improved autophagic clearance of collagen (53). Increased clearance of collagen type I by either WFA or collagen type I siRNA decreased invasiveness of IPF fibroblasts. Collagen type I regulates invasiveness of cells by various mechanisms in IPF (50, 51, 54, 55). Collagen interacts with integrin (56, 57), which can affect invasiveness of the cells in ECM (58). Collagen I secretion and crosslinking increase aberrant integrin signaling in IPF (28, 54), which is responsible for enhanced invasiveness (54, 59). Endogenous increases in collagen I can induce expression of the transcription factor Snail, which is recognized to promote cellular invasion (60).

WFA was used to support the role of VimIF-regulated autophagy in vivo, in a murine model of bleomycin-induced lung fibrosis. Bleomycin increased expression of beclin 1 but increased p62 accumulation, suggesting the lack of autophagy (61). WFA treatment in bleomycin-exposed mice demonstrated further increases in beclin 1 and LC3B expression with decreased p62 expression that correlated with decreased collagen deposition. WFA increased autophagic flux, as evidenced by decreased p62 accumulation in

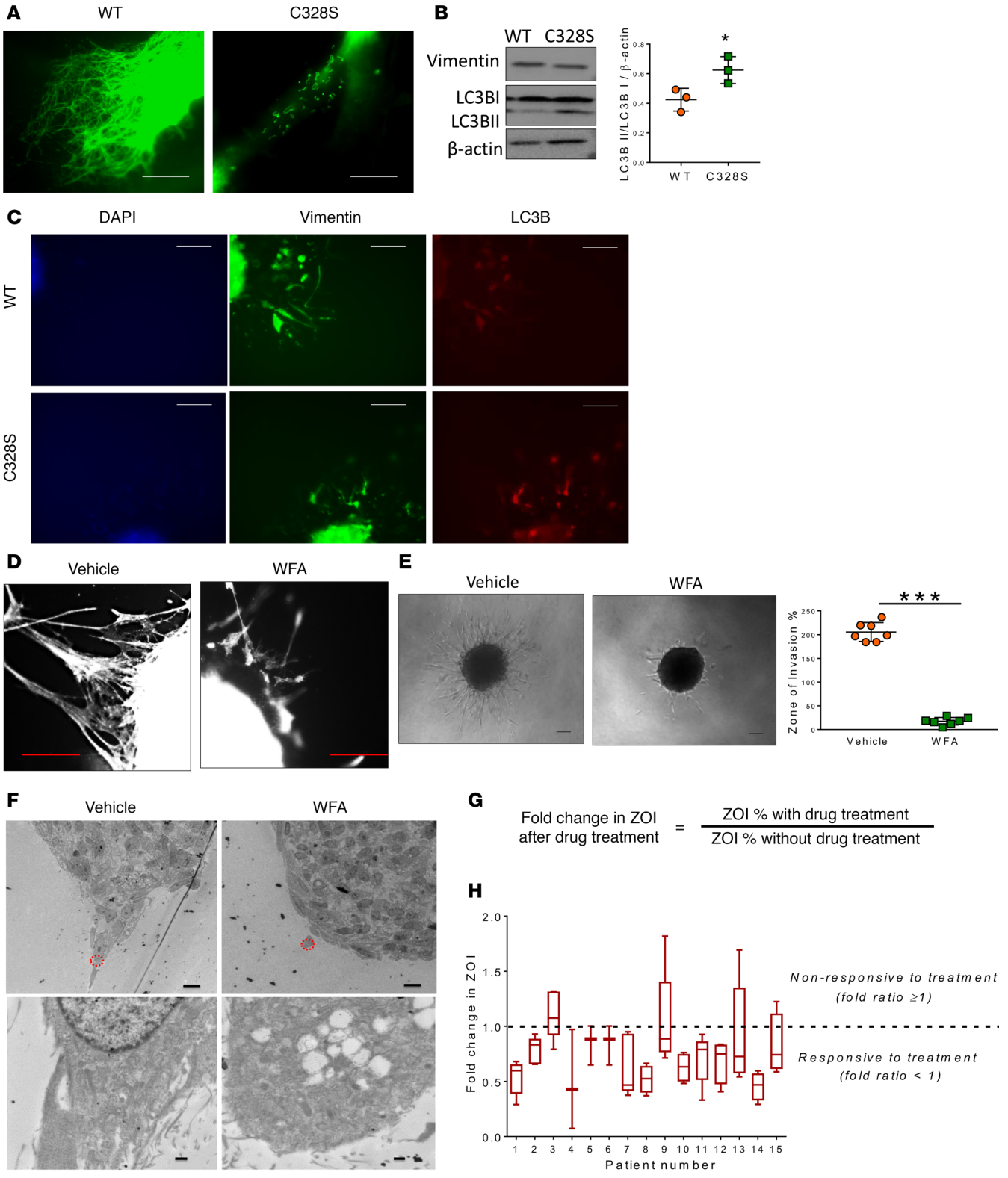

Figure 7. Induction of autophagy by inhibition of VimIF assembly decreases invasiveness. Stable transfection with mEmerald-vimentin construct (WT) and GFP-vimentin-C328S construct (C328S) in Vim$^{-/-}$ mouse fibroblasts. (**A**) Fluorescence images showing arrangement of vimentin in WT and C328S fibroblasts. Scale bars: 50 μm. (**B**) Immunoblot analysis for LC3B and vimentin in transfected fibroblasts after 6 hours of serum starvation. β-Actin served as loading control. Densitometry data are representative of 3 experiments. (**C**) Immunofluorescence staining of pulmospheres using WT and C328 fibroblasts for LC3B (red) and green fluorescence–tagged vimentin expression after 6 hours of serum starvation. Scale bars: 100 μm. (**D**) Fluorescence images of IPF pulmospheres containing mEmerald-vimentin–transfected IPF fibroblasts treated with vehicle (control) or WFA. Scale bars: 250 μm. (**E**) Representative image of pulmospheres treated with vehicle or WFA. Graph shows calculated zone of invasion percentage from 6 IPF lung pulmospheres from controls not treated and treated with WFA. Each dot represents the mean value of calculated zone of invasion

from 5 pulmospheres for each IPF subject. Data are expressed as mean ± SEM. ***P = 0.002, compared with vehicle-treated pulmospheres. (**F**) Transmission electron microscopy images of vehicle- and WFA-treated pulmospheres. Scale bars: 2 μm; magnified images, 500 nm. (**G**) Calculation formula for determination of fold change ratio for zone of invasion (ZOI) area. Median values of ZOI ≥1 represent pulmospheres nonresponsive to the treatment with WFA, and median values of ZOI <1 represent pulmospheres responsive to WFA treatment. (**H**) Invasiveness of pulmospheres from an individual patient not treated and treated with WFA. Box-and-whisker plots for IPF patient pulmospheres treated with WFA. Whiskers show maximum to minimum values. Lines in boxes represent median values.

WFA-treated bleomycin-exposed mice. The data also demonstrate less collagen deposition in mouse lungs after WFA treatment in bleomycin-exposed mice. This increase in autophagy-dependent collagen degradation is also reported in other studies (53, 62). Increased autophagy and decreased invasiveness in pulmospheres obtained from WFA-treated bleomycin-exposed mice demonstrated that induction of autophagy inhibited invasiveness. These results and those of other studies demonstrated that autophagy indirectly regulates cellular invasiveness (63).

We used a genetic approach to assess whether effects of WFA on autophagy are primarily associated with disruption of VimIF assembly. $Vim^{-/-}$ fibroblasts transfected with a fluorescent vimentin C328S construct expressed only squiggle-and-dot forms of vimentin. Cellular stress such as serum starvation increased autophagy in C328S-transfected fibroblasts as compared with fibroblasts transfected with full-length vimentin plasmid, indicating that an intact vimentin network is necessary for autophagy inhibition.

We have previously described a 3D model of human lung organoids to predict the invasive response of IPF fibroblasts to therapy with antifibrotic drugs (9). 3D lung pulmospheres were used in the present study to evaluate the role of WFA in modulating VimIF and fibroblast autophagy in IPF. We noted the presence of vesicles in invasive fibroblasts after treatment with WFA, demonstrating increased autophagy in the fibroblasts. Electron micrographs confirmed the presence of autophagosomes in the fibroblasts of IPF pulmospheres. Linear VimIF assembly was clearly seen in the invading edge of cells, which was inhibited in the WFA-treated cells. Importantly, pulmospheres prepared from 15 IPF patients following lung biopsies were treated with WFA. Cellular invasion was inhibited in these pulmospheres following treatment with WFA. These data demonstrated the ability of WFA to mitigate the loss of autophagy and the subsequent increased invasiveness of IPF fibroblasts.

The IPF fibroblast is characterized by its capacity for enhanced invasion, a cellular property that is being increasingly recognized and studied. Notably, vimentin regulates the invasive capacity of IPF lung fibroblasts through increased assembly of VimIFs. The present study expands the role of vimentin as a regulator of fibroblast invasion and cellular autophagy in IPF. Modulating the assembly of VimIFs may lend itself to therapeutic targeting in pulmonary fibrosis.

Methods

Preparation of lung cells. Lung biopsies (approximately 6 mm × 6 mm) from patients with IPF or control subjects were washed with cold PBS solution. The tissue was incubated with 5 ml collagenase A in a 50-ml tube for 30 minutes in a 37°C water bath. The tube was gently agitated for a few seconds every 10 minutes during this incubation. PBS (20 ml) was added to the tube after 30 minutes of incubation. The tube was then vigorously shaken for 30 seconds to dissolve the tissue, and the resulting suspension was filtered through a 100-μm strainer. The filtered cell suspension was centrifuged for 5 minutes at 300 *g*. The cell pellet was washed with complete DMEM and then resuspended in 10 ml complete DMEM and plated into a gelatin-coated T-25 tissue culture flask. Passage 0–1 cells were used for the preparation of pulmospheres.

Preparation of pulmospheres. Cells were seeded into HEMA-coated (5 mg/ml made in 95% ethanol) 96-well U-bottom plates in complete culture medium consisting of DMEM with penicillin and streptomycin, GlutaMAX, and 5% fetal calf serum (Invitrogen). Plates were spun down for 1 minute at 200 *g* and incubated at 37°C in an incubator in CO_2 overnight. IPF and control pulmospheres were treated with WFA at 1 μM for 12 hours.

Invasion assay. Pulmosphere invasion assay was performed as described earlier (9). Collagen solution was prepared by mixing 2.1 ml precooled (at 4°C) collagen type I solution (3.98 mg/ml) (Corning) and 6.2 ml DMEM (Invitrogen). NaOH (1 M) was used to set a pH of 7–7.4 for this collagen-DMEM solution. 50 μl/well of this solution was added to cover the bottom of flat-bottom 96-well plates and incubated at 37°C in a CO_2 incubator for 2 hours. Single pulmospheres were seeded onto collagen-coated wells with 100 μl

collagen-DMEM solution with WFA (1 μM) or medium alone without WFA. These plates were incubated for 30 minutes at 37°C. 50 μl DMEM with or without WFA was added to each well. Plates were incubated at 37°C in a CO_2 incubator overnight. Images were acquired with a Zeiss Axiocam color camera and analyzed using AxioVision LE Imaging System software (Zeiss).

In the AxioVision LE Imaging System software, the area covered by the invading cells (*H*) was selected and measured. The central mass of the pulmosphere (*R*) was outlined and measured. The percent total invaded area was calculated by $(H - R)/R$*100. Percent invasion area was calculated for 3–5 pulmospheres per sample.

Primary human lung fibroblast isolation. Mixed primary cells from single-cell suspensions obtained from human lungs (as described in *Preparation of lung cells*) were used to isolate primary human lung fibroblasts. These cells were maintained in medium consisting of DMEM (Life Technologies) supplemented with 10% FBS (Sigma-Aldrich), 100 U/ml penicillin/streptomycin (Sigma-Aldrich), and Fungizone (Life Technologies). Fibroblasts were purified by repeat trypsinization and passaging to achieve a homogenous population of spindle cells that uniformly expressed the collagen cross-linking enzyme prolyl 4-hydroxylase. Cell lysates were obtained for Western blot analyses at passages 4–6 and confluence of 90%–100%. IPF fibroblasts were treated with WFA at 1 μM for 12 hours.

Plasmids and transfections. mEmerald-vimentin plasmid was used for localization of vimentin intermediate filament. mEmerald-Vimentin-7 (WT) was a gift from Michael Davidson (Addgene plasmid 54299). The GFP–vimentin C328S construct, in which Cys328 is mutated to serine, is not competent for assembly in vimentin-deficient cells and has been previously described (25). These constructs are referred to as WT and C328S herein. The cells were transfected with plasmid using X-tremeGENE 9 (Sigma-Aldrich). The transfection reactions were performed as per the manufacturer's instructions. Briefly, the transfections were performed in a 24-well plate. The transfection reagent complex was prepared in 1:2 ratio for FuGENE 9 and plasmid, respectively. The reaction was performed in OptiMEM medium (Gibco) for 24 hours. The plasmid-positive fibroblasts were sorted with FACS for GFP. For generation of stably transfected cells, selection was carried out by culture in the presence of 500 μg/ml G-418 (Gibco). GFP-positive FACS-sorted cells were used for preparation of WT and C328S pulmospheres.

For the preparation of mEmerald-Vimentin-7 pulmospheres, human lung fibroblasts were transfected and sorted as above and mixed with the rest of the lung cells. This mixture of cells was used to image immunofluorescence for VimIF in IPF pulmospheres.

For Collagen type I and beclin 1 siRNA studies, we transfected IPF fibroblasts with siRNA targeting collagen I (Santa Cruz Biotechnology) or nontargeting control siRNA (100 nM) using Lipofectamine 2000 reagent (Invitrogen). OptiMEM medium was used for transfection reactions. Transfected cells were treated with or without WFA for 12 hours. These cells were used for the preparation of pulmospheres and Western blot analysis.

Immunofluorescence microscopy. Pulmospheres seeded in collagen were fixed with 4% paraformadehyde for 1 hour at room temperature. Pulmospheres were transferred to Richard-Allan Scientific HistoGel and processed for preparation of paraffin block and sectioning. Deparaffinization and antigen retrieval were performed on paraffin-embedded lung tissue sections. After blocking in PBST (0.1% Triton X-100 in PBS) containing 3% BSA (Sigma-Aldrich) overnight at 4°C and washing in PBST (2 × 15 minutes), pulmospheres were incubated with vimentin antibody (Santa Cruz Biotechnology) diluted in PBST on a gently rocking rotator at 4°C overnight and rinsed in PBST (4 × 5 minutes). When necessary, pulmospheres were then incubated in appropriate Alexa Fluor–conjugated secondary antibodies (Molecular Probes, Life Technologies) for 2 hours at room temperature. Cell nuclei were counterstained by DAPI (Invitrogen) diluted 1:500 in PBS for 10 minutes at room temperature.

For mEmerald-vimentin plasmid-positive (Addgene) pulmospheres, the single-cell suspension was mixed with the mEmerald-vimentin plasmid fibroblasts isolated from the same lung sample.

Immunofluorescence staining on lung sections and fibroblasts was performed as described previously (64). The LC3 puncta per cell quantification was performed using a custom-written ImageJ (NIH) macro containing plug-ins (65).

FACS. Collagen gels containing pulmospheres were digested with Collagenase/Dispase (1 mg/ml) (catalog 10269638001, Roche) solution to obtain pulmosphere cells in cell suspension. The cell suspension was centrifuged for 5 minutes at 1300 rpm and washed for 5 minutes with 1× PBS. Sample was treated with 0.25% trypsin-EDTA for 5 minutes to obtain single-cell suspension. The cell suspension was centrifuged for 5 minutes at 1300 rpm and washed for 5 minutes with 1× PBS twice. Cells were fixed, permeabilized,

and labeled with Alexa Fluor 488–tagged vimentin antibody. Labeled cells were analyzed by FACS, and data were computed using software (BD CellQuest). Gating was performed on the basis of negative control staining profiles, obtained by substituting primary antibodies with isotypic nonimmune IgG.

Western blot analysis. For solubilization of vimentin, cells were lysed in EMPIGEN lysis buffer (20 mM HEPES pH 7.5, 120 mM NaCl, 1 mM EDTA, 2.8% EMPIGEN BB (Sigma-Aldrich), 1× Halt Phosphatase Inhibitor Cocktail (Pierce), and 1× Protease Inhibitor Cocktail (Roche). Cells were washed with ice-cold PBS, and the pellets were snap-frozen in liquid nitrogen. EMPIGEN–protease inhibitor cocktail mixture was used to triturate the frozen pellets. The cell lysate was centrifuged at 12,000 rpm and supernatant was used as protein lysates. Protein concentrations were determined using the Pierce BCA Protein Assay Kit (Thermo Fisher Scientific). Protein samples (15 μg) were prepared in NuPAGE LDS sample buffer (Life Technologies) containing 5% DTT, denatured at 95 °C for 10 minutes, electrophoresed on 4-12% gradient gels (Bio-Rad Criterion gels) using 1× SDS Running Buffer (Bio-Rad), and then transferred to a PVDF membrane (Immobilon-P; Millipore) in transfer buffer containing 25 mM Tris, 192 mM glycine, and 20% methanol (v/v). Membranes were washed with TBS for 5 minutes and incubated in blocking buffer (5% BSA in TBS with 0.1% Tween-20) for 2 hours at room temperature with gentle agitation. Membranes were incubated with anti–beclin 1 (1:1000) (CST-3738, Cell Signaling Technology), anti-LC3B (1:1000) (CST-3868, Cell Signaling Technology), or monoclonal rabbit anti-p62 antibodies (CST-5114 Cell Signaling Technology), and monoclonal mouse anti–β-actin (1:1000) (Sigma-Aldrich) or polyclonal rabbit anti-vimentin (1:500) (sc-5565, Santa Cruz Biotechnology) antibodies in blocking buffer overnight at 4°C. Then, membranes were washed 5 times with washing buffer (TBS with 0.1% Tween-20) (5 minutes each) and probed with the secondary antibody (HRP-conjugated anti-mouse or anti-rabbit IgG antibody; Sigma-Aldrich) at a dilution of 1:5000 for 1 hour at room temperature. Then, membranes were washed 5 times with washing buffer (as above). Membranes were incubated in Immobilon Western Chemiluminescent HRP substrate (Millipore) for 1–2 minutes at room temperature. Blots were scanned using a Bio-Rad image system.

Immunoprecipitation studies. For analysis of endogenous protein interactions, 150-mm dishes of fibroblasts were used to generate whole cell lysates. For solubilization of vimentin, cells were lysed in EMPIGEN lysis buffer (20 mM HEPES pH 7.5, 120 mM NaCl, 1 mM EDTA, 2.8% EMPIGEN BB [Sigma-Aldrich], 1× Halt Phosphatase Inhibitor Cocktail [Pierce], and 1× Protease Inhibitor Cocktail [Roche]). EMPIGEN lysates were rotated at 4°C for at least 30 minutes, and then the soluble fraction was isolated by centrifugation at 20,800 *g* for 10 minutes at 4°C. Lysates were the diluted to 2% EMPIGEN with lysis buffer without detergent prior to addition of the primary antibody. For analysis of the effects of starvation on coimmunoprecipitation, cells were incubated in starvation or normal medium for 6 hours immediately prior to harvesting. Anti–beclin 1 (sc-48341, Santa Cruz Biotechnology) was added to the lysates and rotated for at least 4 hours at 4°C, and then 20–60 μl of a Protein G sepharose slurry (50% v/v) (Santa Cruz Biotechnology) was added for at least 1 hour. Immunoprecipitates were washed 3 times with cold lysis buffer. Whole cell lysates and immunoprecipitated proteins were boiled in 30–40 μl sample buffer and separated by SDS-PAGE on precast 4-15% gels (Bio-Rad).They were transferred and blotted with the monoclonal mouse beclin 1 antibody (sc-48341, Santa Cruz Biotechnology), monoclonal mouse anti-vimentin antibody (sc-6260, Santa Cruz Biotechnology), and monoclonal rabbit LC3B antibody (1:1000) (catalog 3868, Cell Signaling Technology).

Detection of autophagic flux. Formation of autophagosome and autophagolysosomes in WFA-treated IPF fibroblasts was detected using the Premo Autophagy Tandem Sensor RFP-GFP-LC3B Kit (Thermo Fischer Scientific) as described in the manufacturer's instructions. The RFP-GFP-LC3B sensor enables detection of LC3B-positive, neutral-pH autophagosomes in green fluorescence (GFP) and LC3B-positive acidic pH autophagolysosome in red fluorescence (RFP). The cells were grown on coverslips and incubated with 6 μl BacMam Reagents containing the RFP-GFP-LC3B overnight. The cells were then treated with either vehicle alone or WFA at 1 μM for 16 hours. The cells were rinsed in 1× PBS, and nuclei were stained with DAPI. The coverslips were mounted with VECTASHIELD reagent (Vector Laboratories), and fluorescence images were taken using confocal microscopy (Carl Zeiss Meditec Inc.).

IHC. Formalin-fixed, paraffin-embedded lung tissues were used in IHC performed with a Dako EnVision Visualization System, following the manufacturer's standard protocol. Sections were stained with primary Abs against vimentin (1:500) or collagen type I (1:400; both from Santa Cruz Biotechnology). Sections were also stained using a Picro Sirius Red Stain Kit (Abcam) for evaluation of collagen types I and III. For IHC, an Axiovert 200M light microscope was used (×20 lens, numerical aperture 1.3; Zeiss), at room

temperature, with glass slides and bright-field fluorochromes. Images were captured using a QImaging QIClick camera and QCapture Pro version 7 software (QImaging).The staining intensity of IHC staining for vimentin in IPF lung tissues was quantitated using the Fiji version of ImageJ Image Analysis software plug-in developed by the University of Auckland.

Transmission electron microscopy. Transmission electron microscopy of primary lung fibroblasts and pulmospheres was performed in the High Resolution Imaging Shared Facility at UAB. Cells grown on plastic dishes were rinsed in PBS and then fixed overnight at 4°C in 2% glutaraldehyde in 0.1 M sodium cacodylate buffer, pH 7.4. Cells harvested by scraping were pelleted by centrifugation and osmicated for 60 minutes at 4°C in 1% osmium tetroxide in 0.1 M sodium cacodylate buffer. Following the wash with Na cacodylate buffer to remove osmium, samples were stained en bloc with 2% aqueous uranyl acetate for 30 minutes. Following dehydration in graded alcohol, pellets were embedded in Epon 812 and cured at 60°C overnight. Sections (80 nm thick) were generated with a Leica UC6 ultramicrotome (Leica Microsystems), collected on 200 mesh copper grids, and stained in 50% alcoholic uranyl acetate and Reynold's lead citrate. Air-dried grids of both fixed cell lines and clinical biopsy samples were subsequently examined on an FEI Tecnai-T12 electron microscope. Images were collected using a Hamamatsu CCD camera (Hamamatsu Photon).

For TEM of pulmospheres, collagen gel–embedded pulmospheres were harvested and washed in PBS. The rest of the procedure was similar to the processing for fibroblasts as described above.

In vivo studies. We administered intratracheal bleomycin (0.025 U) to C57BL/6J mice (6–8 weeks of age; The Jackson Laboratory) to induce lung injury as previously described (54). For evaluation of the in vivo antifibrotic effects of WFA, WFA (2 mg/kg body weight, DMSO 0.1% v/v) was injected intraperitoneally daily from day 8 to day 21 after bleomycin administration. The control groups were injected with vehicle (DMSO 0.1% v/v). Mice were imaged for microCT scan on day 20. The same groups of mice were sacrificed on day 21 to harvest lungs for further analyses.

129S-Vimtm1Cba/MesDmarkJ mice ($Vim^{-/-}$ mice) were purchased from the Jackson Laboratory for plasmid transfection studies. Fibroblasts from mouse lungs were isolated as described.

MicroCT imaging. To study the progression of lung fibrosis and efficacy of WFA, the experimental mice were subjected to microCT imaging. Control and test animals were imaged under anesthesia in supine position on day 20 following bleomycin administration. The raw files were processed using ImageJ software.

Statistics. Results are presented as mean ± SD, unless specified otherwise. Comparisons between any 2 groups were performed using 2-tailed unpaired Student's *t* tests. Differences were considered statistically significant at $P < 0.05$.

Study approval. Through the UAB interstitial lung disease (ILD) clinic, patients were recruited who were undergoing video-assisted thoracic surgery (VATS) lung biopsies as directed by their treating physicians. Control patients were recruited from those referred to the thoracic surgery clinic who were undergoing a VATS procedure for the removal of a nonmalignant lung nodule. The control biopsy was obtained from an uninvolved lobe during VATS. The UAB IRB approved the protocols. The diagnosis of IPF was based on standard criteria made by clinical information, physical and chest radiographic findings, and histological evaluations (66). UAB Committee on the Use and Care of Animals approved the mouse protocols.

Author contributions

RS designed, conducted experiments, acquired data, analyzed data, and wrote the manuscript. FJL, ZW, and HL conducted processing of lung samples and experiments. KD, VT, SM, and MA discussed the implications and edited the manuscript. DPS provided experimental and conceptual advice and edited the manuscript. VJT gave conceptual advice and edited the manuscript. VBA conceived and designed the study, discussed results and their implications, and edited the manuscript.

Acknowledgments

The authors thank the UAB High Resolution Imaging Shared Facility for help with transmission electron microscopy. This research was supported by NIH grants P01 HL114470 (to VJT and VBA), U54 ES30246 (to MA and VBA), MINECO/FEDER SAF2015-68590-R (to DPS), and R01 ES029981 (to VBA).

Address correspondence to: Veena B. Antony, 1530 3rd Avenue South, THT-541, Birmingham, Alabama 35294, USA. Phone: 205.975.3255; Email: vantony@uabmc.edu.

1. Ahluwalia N, Shea BS, Tager AM. New therapeutic targets in idiopathic pulmonary fibrosis. Aiming to rein in runaway wound-healing responses. *Am J Respir Crit Care Med*. 2014;190(8):867–878.
2. Wolters PJ, Collard HR, Jones KD. Pathogenesis of idiopathic pulmonary fibrosis. *Annu Rev Pathol*. 2014;9:157–179.
3. Basset F, Ferrans VJ, Soler P, Takemura T, Fukuda Y, Crystal RG. Intraluminal fibrosis in interstitial lung disorders. *Am J Pathol*. 1986;122(3):443–461.
4. White ES, et al. Integrin alpha4beta1 regulates migration across basement membranes by lung fibroblasts: a role for phosphatase and tensin homologue deleted on chromosome 10. *Am J Respir Crit Care Med*. 2003;168(4):436–442.
5. Torry DJ, Richards CD, Podor TJ, Gauldie J. Anchorage-independent colony growth of pulmonary fibroblasts derived from fibrotic human lung tissue. *J Clin Invest*. 1994;93(4):1525–1532.
6. Lovgren AK, et al. β-arrestin deficiency protects against pulmonary fibrosis in mice and prevents fibroblast invasion of extracellular matrix. *Sci Transl Med*. 2011;3(74):74ra23.
7. Li Y, et al. Severe lung fibrosis requires an invasive fibroblast phenotype regulated by hyaluronan and CD44. *J Exp Med*. 2011;208(7):1459–1471.
8. Suganuma H, Sato A, Tamura R, Chida K. Enhanced migration of fibroblasts derived from lungs with fibrotic lesions. *Thorax*. 1995;50(9):984–989.
9. Surolia R, et al. 3D pulmospheres serve as a personalized and predictive multicellular model for assessment of antifibrotic drugs. *JCI Insight*. 2017;2(2):e91377.
10. Li H, et al. Anti-microRNA-378a enhances wound healing process by upregulating integrin beta-3 and vimentin. *Mol Ther*. 2014;22(10):1839–1850.
11. Rogel MR, Soni PN, Troken JR, Sitikov A, Trejo HE, Ridge KM. Vimentin is sufficient and required for wound repair and remodeling in alveolar epithelial cells. *FASEB J*. 2011;25(11):3873–3883.
12. Eckes B, et al. Impaired wound healing in embryonic and adult mice lacking vimentin. *J Cell Sci*. 2000;113(Pt 13):2455–2462.
13. Das SK, et al. Vimentin knockdown decreases corneal opacity. *Invest Ophthalmol Vis Sci*. 2014;55(7):4030–4040.
14. dos Santos G, et al. Vimentin regulates activation of the NLRP3 inflammasome. *Nat Commun*. 2015;6:6574.
15. Li FJ, et al. Autoimmunity to vimentin is associated with outcomes of patients with idiopathic pulmonary fibrosis. *J Immunol*. 2017;199(5):1596–1605.
16. Li FJ, et al. Low-dose cadmium exposure induces peribronchiolar fibrosis through site-specific phosphorylation of vimentin. *Am J Physiol Lung Cell Mol Physiol*. 2017;313(1):L80–L91.
17. Araya J, et al. Insufficient autophagy in idiopathic pulmonary fibrosis. *Am J Physiol Lung Cell Mol Physiol*. 2013;304(1):L56–L69.
18. O'Dwyer DN, Ashley SL, Moore BB. Influences of innate immunity, autophagy, and fibroblast activation in the pathogenesis of lung fibrosis. *Am J Physiol Lung Cell Mol Physiol*. 2016;311(3):L590–L601.
19. Mora AL, Bueno M, Rojas M. Mitochondria in the spotlight of aging and idiopathic pulmonary fibrosis. *J Clin Invest*. 2017;127(2):405–414.
20. Kuwano K, et al. Cellular senescence and autophagy in the pathogenesis of chronic obstructive pulmonary disease (COPD) and idiopathic pulmonary fibrosis (IPF). *Respir Investig*. 2016;54(6):397–406.
21. Bueno M, et al. PINK1 deficiency impairs mitochondrial homeostasis and promotes lung fibrosis. *J Clin Invest*. 2015;125(2):521–538.
22. Im J, Hergert P, Nho RS. Reduced FoxO3a expression causes low autophagy in idiopathic pulmonary fibrosis fibroblasts on collagen matrices. *Am J Physiol Lung Cell Mol Physiol*. 2015;309(6):L552–L561.
23. Sosulski ML, Gongora R, Danchuk S, Dong C, Luo F, Sanchez CG. Deregulation of selective autophagy during aging and pulmonary fibrosis: the role of TGFβ1. *Aging Cell*. 2015;14(5):774–783.
24. Kast DJ, Dominguez R. The cytoskeleton-autophagy connection. *Curr Biol*. 2017;27(8):R318–R326.
25. Pérez-Sala D, Oeste CL, Martínez AE, Carrasco MJ, Garzón B, Cañada FJ. Vimentin filament organization and stress sensing depend on its single cysteine residue and zinc binding. *Nat Commun*. 2015;6:7287.
26. Bargagna-Mohan P, et al. The tumor inhibitor and antiangiogenic agent withaferin A targets the intermediate filament protein vimentin. *Chem Biol*. 2007;14(6):623–634.
27. Jones MG, et al. Three-dimensional characterization of fibroblast foci in idiopathic pulmonary fibrosis. *JCI Insight*. 2016;1(5).
28. Chen H, et al. Mechanosensing by the α6-integrin confers an invasive fibroblast phenotype and mediates lung fibrosis. *Nat Commun*. 2016;7:12564.
29. Ahluwalia N, et al. Fibrogenic lung injury induces non-cell-autonomous fibroblast invasion. *Am J Respir Cell Mol Biol*. 2016;54(6):831–842.
30. Geng J, et al. Phosphatase and tensin homolog deleted on chromosome 10 contributes to phenotype transformation of fibroblasts in idiopathic pulmonary fibrosis via multiple pathways. *Exp Biol Med (Maywood)*. 2016;241(2):157–165.
31. Chang L, Goldman RD. Intermediate filaments mediate cytoskeletal crosstalk. *Nat Rev Mol Cell Biol*. 2004;5(8):601–613.
32. Goldman RD, Cleland MM, Murthy SN, Mahammad S, Kuczmarski ER. Inroads into the structure and function of intermediate filament networks. *J Struct Biol*. 2012;177(1):14–23.
33. Lowery J, Kuczmarski ER, Herrmann H, Goldman RD. Intermediate filaments play a pivotal role in regulating cell architecture and function. *J Biol Chem*. 2015;290(28):17145–17153.
34. Wei J, et al. Overexpression of vimentin contributes to prostate cancer invasion and metastasis via src regulation. *Anticancer Res*. 2008;28(1A):327–334.
35. Zhu QS, et al. Vimentin is a novel AKT1 target mediating motility and invasion. *Oncogene*. 2011;30(4):457–470.
36. Helfand BT, et al. Vimentin organization modulates the formation of lamellipodia. *Mol Biol Cell*. 2011;22(8):1274–1289.
37. Schoumacher M, Goldman RD, Louvard D, Vignjevic DM. Actin, microtubules, and vimentin intermediate filaments cooperate for elongation of invadopodia. *J Cell Biol*. 2010;189(3):541–556.
38. Sibony-Benyamini H, Gil-Henn H. Invadopodia: the leading force. *Eur J Cell Biol*. 2012;91(11-12):896–901.
39. Eckes B, et al. Impaired mechanical stability, migration and contractile capacity in vimentin-deficient fibroblasts. *J Cell Sci*. 1998;111(Pt 13):1897–1907.
40. Terriac E, et al. Vimentin levels and serine 71 phosphorylation in the control of cell-matrix adhesions, migration speed, and shape of transformed human fibroblasts. *Cells*. 2017;6(1).

41. Henderson P, Wilson DC, Satsangi J, Stevens C. A role for vimentin in Crohn disease. *Autophagy*. 2012;8(11):1695–1696.
42. Wang RC, et al. Akt-mediated regulation of autophagy and tumorigenesis through Beclin 1 phosphorylation. *Science*. 2012;338(6109):956–959.
43. Nishio K, Inoue A, Qiao S, Kondo H, Mimura A. Senescence and cytoskeleton: overproduction of vimentin induces senescent-like morphology in human fibroblasts. *Histochem Cell Biol*. 2001;116(4):321–327.
44. Frescas D, et al. Senescent cells expose and secrete an oxidized form of membrane-bound vimentin as revealed by a natural polyreactive antibody. *Proc Natl Acad Sci USA*. 2017;114(9):E1668–E1677.
45. Schafer MJ, et al. Cellular senescence mediates fibrotic pulmonary disease. *Nat Commun*. 2017;8:14532.
46. Kidd ME, Shumaker DK, Ridge KM. The role of vimentin intermediate filaments in the progression of lung cancer. *Am J Respir Cell Mol Biol*. 2014;50(1):1–6.
47. Pozuelo-Rubio M. Regulation of autophagic activity by 14-3-3ζ proteins associated with class III phosphatidylinositol-3-kinase. *Cell Death Differ*. 2011;18(3):479–492.
48. Tzivion G, Avruch J. 14-3-3 proteins: active cofactors in cellular regulation by serine/threonine phosphorylation. *J Biol Chem*. 2002;277(5):3061–3064.
49. Kleppe R, Martinez A, Døskeland SO, Haavik J. The 14-3-3 proteins in regulation of cellular metabolism. *Semin Cell Dev Biol*. 2011;22(7):713–719.
50. Hansen NU, Karsdal MA, Brockbank S, Cruwys S, Rønnow S, Leeming DJ. Tissue turnover of collagen type I, III and elastin is elevated in the PCLS model of IPF and can be restored back to vehicle levels using a phosphodiesterase inhibitor. *Respir Res*. 2016;17(1):76.
51. Giménez A, Duch P, Puig M, Gabasa M, Xaubet A, Alcaraz J. Dysregulated collagen homeostasis by matrix stiffening and TGF-β1 in fibroblasts from idiopathic pulmonary fibrosis patients: role of FAK/Akt. *Int J Mol Sci*. 2017;18(11).
52. Challa AA, Stefanovic B. A novel role of vimentin filaments: binding and stabilization of collagen mRNAs. *Mol Cell Biol*. 2011;31(18):3773–3789.
53. Kim SI, Na HJ, Ding Y, Wang Z, Lee SJ, Choi ME. Autophagy promotes intracellular degradation of type I collagen induced by transforming growth factor (TGF)-β1. *J Biol Chem*. 2012;287(15):11677–11688.
54. Zhou Y, et al. Inhibition of mechanosensitive signaling in myofibroblasts ameliorates experimental pulmonary fibrosis. *J Clin Invest*. 2013;123(3):1096–1108.
55. Levental KR, et al. Matrix crosslinking forces tumor progression by enhancing integrin signaling. *Cell*. 2009;139(5):891–906.
56. Kim H, Nakamura F, Lee W, Hong C, Pérez-Sala D, McCulloch CA. Regulation of cell adhesion to collagen via beta1 integrins is dependent on interactions of filamin A with vimentin and protein kinase C epsilon. *Exp Cell Res*. 2010;316(11):1829–1844.
57. Sipilä KH, et al. Proline hydroxylation in collagen supports integrin binding by two distinct mechanisms. *J Biol Chem*. 2018;293(20):7645–7658.
58. Ojalill M, et al. Integrin α2β1 decelerates proliferation, but promotes survival and invasion of prostate cancer cells. *Oncotarget*. 2018;9(65):32435–32447.
59. Gkretsi V, Stylianopoulos T. Cell adhesion and matrix stiffness: coordinating cancer cell invasion and metastasis. *Front Oncol*. 2018;8:145.
60. Shields MA, Dangi-Garimella S, Krantz SB, Bentrem DJ, Munshi HG. Pancreatic cancer cells respond to type I collagen by inducing snail expression to promote membrane type 1 matrix metalloproteinase-dependent collagen invasion. *J Biol Chem*. 2011;286(12):10495–10504.
61. Liu H, et al. SB216763, a selective small molecule inhibitor of glycogen synthase kinase-3, improves bleomycin-induced pulmonary fibrosis via activating autophagy. *Acta Pharmaceutica Sinica B*. 2013;3(4):226–233.
62. Yang HZ, et al. TLR4 activity is required in the resolution of pulmonary inflammation and fibrosis after acute and chronic lung injury. *Am J Pathol*. 2012;180(1):275–292.
63. Luo X, Cheng W, Wang S, Chen Z, Tan J. Autophagy suppresses invasiveness of endometrial cells through reduction of fascin-1. *Biomed Res Int*. 2018;2018:8615435.
64. Karki S, et al. Wilms' tumor 1 (Wt1) regulates pleural mesothelial cell plasticity and transition into myofibroblasts in idiopathic pulmonary fibrosis. *FASEB J*. 2014;28(3):1122–1131.
65. Chu CT, Plowey ED, Dagda RK, Hickey RW, Cherra SJ, Clark RS. Autophagy in neurite injury and neurodegeneration: in vitro and in vivo models. *Meth Enzymol*. 2009;453:217–249.
66. An official ATS/ERS/JRS/ALAT Clinical Practice Guideline: treatment of idiopathic pulmonary fibrosis. An Update of the 2011 Clinical Practice Guideline. *Am J Respir Crit Care Med*. 2015;192(5):644.